

# Mechanism for nonequilibrium symmetry breaking and pattern formation in magnetic films

J. M. Deutsch and Trieu Mai

*Department of Physics, University of California, Santa Cruz, California 95064, USA*

(Dated: March 2, 2022)

Magnetic thin films exhibit a strong variation in properties depending on their degree of disorder. Recent coherent x-ray speckle experiments on magnetic films have measured the loss of correlation between configurations at opposite fields and at the same field, upon repeated field cycling. We perform finite temperature numerical simulations on these systems that provide a comprehensive explanation for the experimental results. The simulations demonstrate, in accordance with experiments, that the memory of configurations increases with film disorder. We find that non-trivial microscopic differences exist between the zero field spin configuration obtained by starting from a large positive field and the zero field configuration starting at a large negative field. This seemingly paradoxical behavior is due to the nature of the vector spin dynamics and is also seen in the experiments. For low disorder, there is an instability which causes the spontaneous growth of line-like domains at a critical field, also in accord with experiments. It is this unstable growth, which is highly sensitive to thermal noise, that is responsible for the small correlation between patterns under repeated cycling. The domain patterns, hysteresis loops, and memory properties of our simulated systems match remarkably well with the real experimental systems.

PACS numbers:

## I. INTRODUCTION

Many magnetic systems have a memory of their past configurations. This history, manifest in the hysteresis loop of a magnet, has many fascinating features, for example Barkhausen noise which demonstrates that this history has intricate behavior at a small scale, with avalanches occurring in the same order in a highly reproducible manner [1, 2, 3, 4, 5, 6, 7, 8]. From a theoretical perspective, a certain class of Ising models has been proved by Sethna *et al.* [9] to exhibit perfect return point memory [27] And of course, hysteresis is the principle that makes magnetic storage devices possible [10].

Primarily due to the technological importance of magnetic systems, a vast number of experiments have been done to observe magnetic memory and hysteresis phenomena [10]. A comparably large number of theories have been made to explain these experiments with varying degrees of success. A recent experiment by Pierce *et al.* [11, 12] measured the memory properties of magnetic multilayer thin films. They observed an effect that at first sight appears paradoxical, involving fundamental issues of symmetry in these systems. In this paper, through numerical simulations, we attempt to provide an explanation for this effect.

The experiment by Pierce *et al.* used the powerful new tool of x-ray speckle metrology to measure the covariance of a domain configuration at one field with the configuration at another field. This measured value is one way to quantify the amount of “memory” possessed by the material. Measurements were done for Co/Pt multilayer samples with varying amounts of disorder; the study found that samples with greater disorder had higher “memory” than the ordered samples which showed no significant amount of memory. The domain patterns ranged

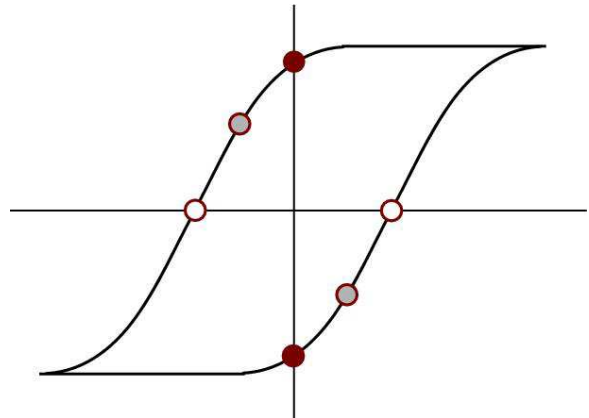


FIG. 1: Magnetization vs. external field for a cartoon hysteresis system. Return point memory is defined as the covariance between any point with the same point after an integer number of complete cycles. Complementary points are points lying a half-integer number of field cycles away. Each pair of points (filled, shaded, and unfilled) is a pair of complementary points.

from labyrinthine mazes for low disorder samples to ones without any noticeable structure for the highest disorder samples. Hysteresis loops for different samples had dramatically different features depending on the amount of disorder, with steep cliffs (large changes in the magnetization at constant field) existing in the hysteresis loops of the low disorder samples.

In addition to the memory dependence on disorder, an unexpected finding was the difference between what Pierce *et al.* called “return point memory” (RPM) and “complementary point memory” (CPM). RPM was defined by them as the covariance, see below, between the

configuration at a certain field point with the configuration at the same field point after an integer number of complete cycles around the major hysteresis loop. CPM is defined as the covariance between the configuration at a certain field point with the configuration at a half integer number of field cycles away. Figure 1 shows examples of “return” and “complementary” points. The covariance that we will use in order to define RPM and CPM is

$$\text{cov}(a, b) = \langle \mathbf{s}_a(\mathbf{r}) \cdot \mathbf{s}_b(\mathbf{r}) \rangle - \langle \mathbf{s}_a(\mathbf{r}) \rangle \cdot \langle \mathbf{s}_b(\mathbf{r}) \rangle, \quad (1)$$

where  $a$  and  $b$  refer to legs on the hysteresis loop and the average is over all space (spins). The normalized covariance is defined by

$$\rho = \frac{\text{cov}(a, b)}{\sqrt{\text{cov}(a, a)\text{cov}(b, b)}}. \quad (2)$$

At a certain external field  $B_e$ , RPM is defined as  $\rho(B_e, a; B_e, b)$ , where  $a$  and  $b$  are legs going in the same direction (both ascending or both descending), and CPM is defined as  $-\rho(B_e, a; -B_e, b)$ , where  $a$  and  $b$  are legs going in opposite directions. Perfect memory would lead to both RPM and CPM equal to unity. A covariance between two independent systems would approach zero for both RPM and CPM.

The speckle experiment measured intensities from x-ray scattering. Because scattering experiments probe samples in Fourier space, the actual measurements did not measure the covariance as defined by Eq.(1) but instead by

$$\text{cov}_k(a, b) = \langle |s_a^z(\mathbf{k})|^2 |s_b^z(\mathbf{k})|^2 \rangle - \langle |s_a^z(\mathbf{k})|^2 \rangle \langle |s_b^z(\mathbf{k})|^2 \rangle, \quad (3)$$

where  $s_a^z(\mathbf{k})$  is the z component of the Fourier transform of the spins on leg  $a$  and the average is over wave vectors [28]. Using this Fourier space covariance in the definition of RPM and CPM, Pierce *et al.* measured the amount of memory for samples of Co/Pt multilayer thin films with a wide range of disorder. RPM and CPM are both negligible for samples with low disorder and are quite significant ( $\gtrsim 0.6$  at the coercive field) for highly disordered samples. The onset of memory occurs quite abruptly as disorder is increased. Furthermore, for samples with significant memory, RPM is noticeably larger than CPM for all fields measured. In this paper we will use the real space covariance in the definition of RPM and CPM.

A viable model of the Co/Pt multilayer films must at the least be able to explain two experimental results:

1. RPM, CPM  $\sim 0$  for systems with low disorder
2.  $1 > \text{RPM} > \text{CPM}$  for systems with high disorder

In this paper, we provide a possible explanation for these experimental results through finite temperature numerical simulations of classical vector spins. The finite temperature destroys perfect memory and affects both RPM and CPM. We will see that the nature of the domains

determine how much the temperature affects the covariance; highly ordered systems are more susceptible to temperature effects than highly disordered systems, and do explain result I. But thermal noise does not discriminate between the ascending leg and the descending leg. A satisfactory theory must also show that RPM is greater than CPM.

Condition 2 is difficult to understand intuitively. Consider a system at low temperature that starts out fully saturated from being in a large positive external field perpendicular to the film, and then that field is brought down adiabatically to zero. At remanence the system will be in a state with domains pointing in different directions. Now repeat the same procedure but starting with a fully saturating field pointing in the opposite direction. At remanence we now expect the final configuration to be the same apart from a change in sign  $\mathbf{s} \rightarrow -\mathbf{s}$ . The fact that the CPM value is less than the RPM value contradicts this. The configurations although somewhat correlated, are different.

One possible explanation of this can be devised by introducing a term in the Hamiltonian that is not invariant under spin and external field reversal  $\mathbf{s} \rightarrow -\mathbf{s}$  and  $B_e \rightarrow -B_e$ . Terms in this class automatically introduce a difference between the ascending and descending legs. A system with such a Hamiltonian would exhibit a hysteresis loop that is not symmetric under the same operations even at zero temperature. Using a scalar  $\phi^4$  model with a random field term in the Hamiltonian, Jagla [12, 13] was able to satisfy both conditions. But the physical origin, and existence, of these random fields is unclear. Recently, with some modifications to his  $\phi^4$  model, including replacing the random fields with random anisotropy, Jagla [14] was able to produce domain patterns and hysteresis loops that resemble the experimental patterns and loops remarkably well. However without a random field term in the Hamiltonian, the memory conditions could not be satisfied.

We provide a possibly more fundamental mechanism that satisfies condition 2: The vector dynamics breaks the spin and field reversal symmetry, thereby reducing CPM and not RPM. This mechanism does not require any new terms in the Hamiltonian of the class mentioned in the previous paragraph. In our earlier work [15], we showed how the vector dynamics, governed by the Landau-Lifshitz-Gilbert (LLG) equation [16], can give rise to non-complementary hysteresis loops for a system of nanomagnetic pillars. The crucial role of vector dynamics for explaining experimental results underlines the inadequacy of scalar models, even when the system is highly anisotropic. We have not excluded the possibility that the real explanation is a combination of the vector dynamics and the random fields. Furthermore it is possible that the experiments result from some other effects that have not been considered so far. In this paper, we use numerical simulations to demonstrate the plausibility of this vector mechanism.

In the next section of this paper, the LLG equation is

introduced and the various terms in the Hamiltonian and their origin will be described. Details of the numerics are provided in Sec. III and the types of domain patterns and hysteresis loops from these simulations are presented in Sec. IV. Sec. V contains the covariance results.

## II. CLASSICAL SPIN DYNAMICS AND THE MODEL HAMILTONIAN

The Landau-Lifshitz-Gilbert equation of motion [16] is the simplest dynamic equation for classical spins that contains a reactive term and a dissipative term:

$$\frac{d\mathbf{s}}{dt} = -\mathbf{s} \times (\mathbf{B} - \gamma \mathbf{s} \times \mathbf{B}), \quad (4)$$

where  $\mathbf{s}$  is a microscopic classical spin,  $\mathbf{B}$  is the local effective field, and  $\gamma$  is a damping coefficient. The effective field is  $\mathbf{B} = -\partial\mathcal{H}/\partial\mathbf{s} + \boldsymbol{\zeta}$ , where  $\mathcal{H}$  is the Hamiltonian and  $\boldsymbol{\zeta}$  represents the effect of thermal noise. The overall constant in front of the right hand side of Eq.(4) is set to unity.

Both terms on the right hand side of the LLG equation are necessary to adequately describe the motion of classical spins. The double cross product in the damping term is necessary in order to maintain a constant magnitude for the spins. The relaxation time is inversely related to the damping coefficient. The reactive term describes precession of a spin about its local effective field and has a quantum mechanical origin; the commutation relations of angular momentum variables give rise to the single cross product of the reactive term. The commutation relation between spin variables is odd under spin reversal. Later, we will show how precession is crucial to adequately describe the experimental system using our Hamiltonian. Because scalar models cannot have precession, the mechanism that we suggest is not possible in scalar theories.

The LLG equation can be applied to microscopic spins as well as coarse grained spins. Every spin variable in the numerics represents a block spin of the multilayer film and the evolution of all spins is calculated by numerically integrating the LLG equation. Henceforth in this paper, a “spin” corresponds to a block spin variable. The coefficients of the Hamiltonian, the damping coefficient, and thermal noise are also those associated with the coarse grained variables. The Hamiltonian has four terms: self anisotropy energy, local ferromagnetic interactions, long range dipole-dipole interactions, and the energy for the interactions with the external field.

The Co/Pt multilayer film is a perpendicular anisotropic material. We define this perpendicular axis as the  $z$  axis. The origin of the perpendicular easy axis is the layered structure of the material. Any real material will have imperfections in the layering, and this imperfection in the layering is the “disorder” mentioned many times in the previous section. Samples with low disorder show very well defined planes separating the layers

of the two elements, whereas samples with high disorder have very rough interfaces between the Co and Pt. Due to this disorder in the layering, each spin has a different easy axis,  $\hat{\mathbf{n}}_i$ . The anisotropy energy term is described by

$$\mathcal{H}_{ani} = -\alpha \sum_i (\mathbf{s}_i \cdot \hat{\mathbf{n}}_i)^2, \quad (5)$$

where  $\alpha$  is a model parameter. The anisotropy must be an even function due to the symmetry in  $\pm\hat{\mathbf{n}}_i$ . Aside from being even, the functional form of Eq.(5) can be quite complicated in general, but if a power expansion is possible, Eq.(5) would be the leading order term.

The next term in the Hamiltonian describes the local ferromagnetic coupling between neighboring spins,

$$\mathcal{H}_J = -J \sum_{\langle i,j \rangle} \mathbf{s}_i \cdot \mathbf{s}_j, \quad (6)$$

where  $J$  is the ferromagnetic coupling constant. We consider only the  $J > 0$  case. Even though we attempt to model a continuum system, a grid is necessary for the numerics. In order to minimize artificial effects due to the grid, this real space ferromagnetic energy term is replaced by a term in Fourier space of the form

$$\mathcal{H}_{el} = J \sum_{\mathbf{k}} k^2 s_{\mathbf{k}}^2. \quad (7)$$

Eq.(7) is the leading order term of the elastic energy in Fourier space which aligns spins locally similar to  $\mathcal{H}_J$ . Disorder can be introduced in the elastic constant  $J$  as well. For small disorder of this type, the results presented in this paper do not change qualitatively. We eliminate this extra disorder parameter and have a uniform elastic constant for all spins.

In addition to the local interactions, the spins also interact via a long range dipole-dipole energy. The form of this energy is the usual classical expression

$$\mathcal{H}_{dip} = -w \sum_{i,j \neq i} \frac{3(\mathbf{s}_i \cdot \mathbf{e}_{ij})(\mathbf{e}_{ij} \cdot \mathbf{s}_j) - \mathbf{s}_i \cdot \mathbf{s}_j}{r_{ij}^3}, \quad (8)$$

where  $\mathbf{r}_{ij}$  is the displacement vector between spins  $i$  and  $j$ ,  $\mathbf{e}_{ij}$  is the unit vector along this direction, and  $w$  is another model parameter. When the spins are pointing predominantly in the  $\pm z$  directions, the dipolar fields tend to anti-align the spins. This competition with the ferromagnetic interaction produces many of the domain features. Interestingly, when the spins are in-plane, the dipole-dipole and local interactions can become cooperative (depending on  $\mathbf{r}_{ij}$ ).

The form of the dipole energy expressed by Eq.(8) is correct for point dipoles, but must be corrected for the block spins of interest. The small but finite thickness of the layers does not significantly change the long range behavior of Eq.(8), but it does eliminate the divergence at small separations [17]. This cutoff is implemented in

Fourier space which is a more computationally efficient basis to calculate long range dipolar fields. Multiplying a gaussian of the form  $\exp(-k^2 d^2/2)$  to the Fourier transform of Eq.(8) effectively removes the divergence at large wave vectors while retaining the original form for small wave vectors. The model parameter,  $d$ , is the length scale of the cutoff where the finite thickness of the sample affects the dipolar interaction.

The last term in the Hamiltonian is the energy from the interaction of the spins with the external field which we take to be uniform in the  $z$  direction,

$$\mathcal{H}_{ext} = -B_e \sum_i s_i^z. \quad (9)$$

Major hysteresis loops are simulated by cycling the external field from a large positive value (past saturation) to a large negative value and back again. To ensure total saturation we reset the value of the spin variables to point completely along the field direction at the start of each leg in the hysteresis loop.

In summary, the full model Hamiltonian has four terms: anisotropy, ferromagnetic coupling, dipole-dipole interaction, and the external field term as described by Eqs.(5,7-9),

$$\mathcal{H} = \mathcal{H}_{ani} + \mathcal{H}_{el} + \mathcal{H}_{dip} + \mathcal{H}_{ext}. \quad (10)$$

The model Hamiltonian is bilinear in the spins,  $\mathbf{s}_i$  and external field,  $B_e$ , therefore it is symmetric under  $\mathbf{s}_i \rightarrow -\mathbf{s}_i$  and  $B_e \rightarrow -B_e$ . However, as mentioned above, this symmetry does not exist for the equation of motion. Under these two operations, the left hand side of the LLG equation, Eq.(4), and the dissipative term reverse signs, whereas the reactive term stays unchanged. With the symmetric model Hamiltonian and using purely relaxational dynamics, in some sense there would be no way to differentiate from going down the descending leg or up the ascending leg of the hysteresis loop. The difference in sign change between the terms of the LLG equation under spin and field reversal is the mechanism by which  $\text{RPM} > \text{CPM}$ . When precession is turned off, the covariance results presented in Sec. V are no longer valid and we verified that as expected,  $\text{RPM} \simeq \text{CPM}$  when the temperature is non-zero and  $\text{RPM} = \text{CPM} = 1$  identically when there is no thermal noise.

This explanation for why  $\text{RPM} > \text{CPM}$  may become invalid when the relaxation time is much smaller than the precessional period. There is no reason to believe that this is the case for multilayer thin films. In fact,  $\gamma$ , the damping coefficient which is a measure of the relative importance between damping and precession has been measured for NiFe thin films and found to be approximately 0.01 [18]. This indicates that the relaxation time is much larger than the precessional period, thus precession is substantial for some systems. The damping is found to be enhanced to  $\sim 1$  for CoCr/Pt multilayer films [19]. For the numerical simulations, we have set  $\gamma$  to unity.

### III. NUMERICS

We simulate the multilayer thin film by a two dimensional lattice of block vector spins of unit length. Most of the model parameters are noted in the previous section: the relative strengths of the coupling constants in the Hamiltonian,  $\alpha, J$ , and  $w$ , the dipolar cutoff length  $d$ , and the damping coefficient  $\gamma$ . There are two more model parameters, the temperature,  $T$ , and  $\lambda$ , a parameter that controls the variation in the easy axes,  $\hat{\mathbf{n}}_i$ . Each  $\hat{\mathbf{n}}_i$  is assigned randomly for every spin. The stacking of the layers in the  $z$  direction is the physical origin of the anisotropy, therefore the  $\hat{\mathbf{n}}_i$ 's are weighted in this direction. This weighting factor,  $\lambda$ , is inversely related to the amount of disorder.

The large number of parameters may at first seem hopeless from the point of view of prediction because in a seven dimensional parameter space almost any curve can likely be fit. This clearly diminishes the predictive power of a model. All is not lost, because the behavior described in this paper is quite robust in many of these parameters. Furthermore there is agreement, at least at the qualitative level, for all the quantities measured at a fixed value of parameters: the shape of the hysteresis loops as a function of disorder, the evolution at low disorder of patterns in the films which have also been seen experimentally, and the RPM and CPM behavior as a function of disorder. As we mentioned at the beginning of the last section,  $\gamma$  has been measured in a certain multilayer system to be  $\sim 1$  [19], and we have set it equal to unity for all simulations. A smaller  $\gamma$  would almost certainly enhance our results. The dipolar cutoff,  $d$ , determines a length scale of the domains, and all other parameters are considered with respect to this length scale. Without loss of generality, we have set  $d = 4$  lattice spacings. Below, we will report results for different temperature and disorder, therefore  $T$  and  $\lambda$  are not fixed model parameters. That leaves us with a three dimensional parameter space and the task does not seem so daunting as before.

One may ask that since we are simulating a known experimental system, why are we not using measured values for these quantities in our numerics? First, these are not known for these disordered Co/Pt films, and even if this could be done, the simulations are of coarse grained spins and not microscopic spins therefore all coefficients, for example, temperature, magnetic field, disorder strength, would change in a highly nontrivial manner. Lattices of sizes  $128 \times 128$  and  $256 \times 256$  spins are used in the simulations, therefore each block spin represents roughly forty thousand real microscopic spins. Nevertheless, even with only  $128^2$  spins, we are able to observe behavior quite similar to what is seen in the experiments.

Initially, the easy axes,  $\hat{\mathbf{n}}_i$  are independently and randomly assigned for each spin. The  $z$  component is weighted by  $\lambda$  which sets the amount of disorder; disorder is small when  $\lambda$  is large and is increased by decreasing  $\lambda$ . The system is initially saturated in the positive  $z$  direc-

tion. Starting from a large positive external field,  $B_e^{max}$ , the field is adiabatically decreased to a large negative field,  $-B_e^{max}$  and the spins are again saturated. From there, the field is adiabatically increased back to  $B_e^{max}$  to finish one complete field cycle.

At zero temperature, adiabatic field cycling is straightforward: after every field step, the spins evolve in time until the configuration reaches a local minimum in the energy, then the field is changed by another step. With thermal noise, the adiabatic condition cannot be as stringent as it is at absolute zero. The adiabatic condition becomes nontrivial because thermal noise is constantly buffeting the spins. The systems of interest have a large anisotropy with easy axes weighted in the  $z$  direction, therefore the energy minima of the spins are predominantly in the  $\pm z$ -direction. If the temperature is not too large, it would be unlikely for thermal noise to be sufficient to knock the spin over the energy barrier to induce a spin-flip.

We use the fact that thermally activated spin-flips are uncommon to construct an adiabatic condition. The spins are allowed to vary their orientation from the vertical, but if the  $z$  component of any spin changes from greater than a large threshold value to less than the negative of that same value (or vice versa), then the system has not yet satisfied the adiabatic condition. If spin-flip events do occur, the spins must be evolved further without changing the field. This threshold value is set to 0.75 for the results in this paper. Qualitatively similar results are obtained for slightly different thresholds. In addition to not allowing large spin flips for the adiabatic condition, the change of the total magnetization in the  $z$  direction,  $\Delta M$ , must also not change substantially. The condition used is  $\Delta M < 0.1$ .

The time evolution of the spins follows the LLG equation. This is done by calculating the effective field for each spin and then integrating the equations using the fourth order Runge-Kutta algorithm. Due to the long range nature of the dipolar interaction, all the spins are coupled together and a real space numerical integration is  $O(N^2)$ . Using a FFT algorithm, this is reduced to  $O(N \ln N)$ . Periodic boundary conditions are used to accommodate the Fourier method, but the results here should not differ significantly with different boundary conditions.

The configurations of spins are stored at certain fields and RPM and CPM as defined in the first section are calculated between different legs. For efficiency, many legs are run in parallel. In the next section, the domain patterns and hysteresis loops resulting from these numerics are discussed.

#### IV. DOMAIN PATTERNS AND HYSTERESIS LOOPS

Using the numerics described in the previous section, qualitatively different configurations and hysteresis loops

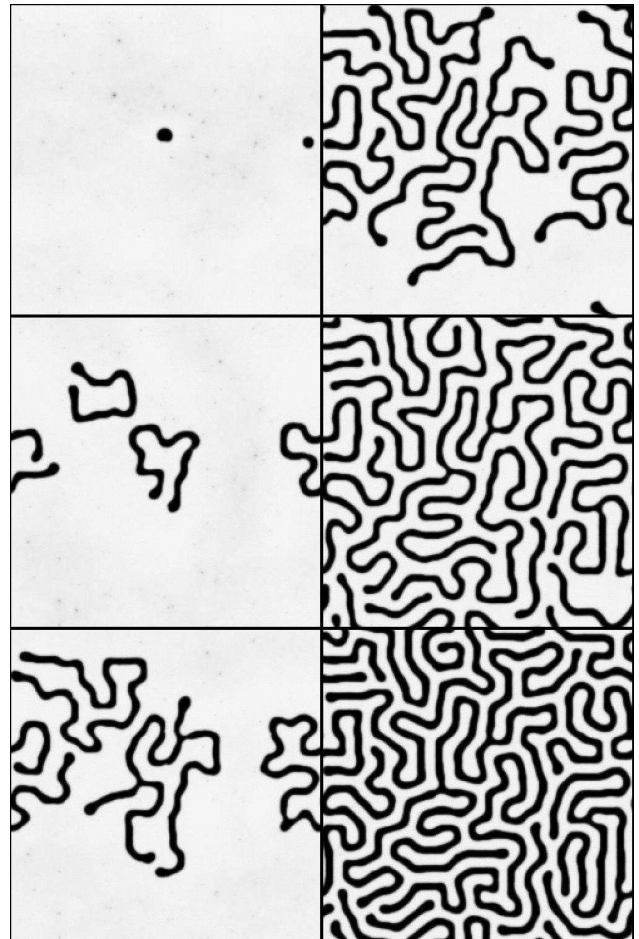


FIG. 2: Domain growth for a  $256^2$  system with low disorder,  $\lambda = 1000$  and  $w = 0.15$ . The  $z$  component of the spins are shown with light shades representing “up” and dark shades representing “down.” The first five panels are at constant field and show snake-like domains growing in time. The labyrinthine patterns resemble the domain patterns of the low disorder samples from the speckle experiments. Eventually, the length of the domains becomes comparable to the system size and require a lowering of the external field to increase in size. The last panel is at a lower external field than the other five.

arise depending on the parameters described in Sec. II. The important parameters are the relative strengths between the interaction terms in the Hamiltonian ( $\alpha$ ,  $J$ , and  $w$ ), and the amount of disorder (characterized by  $\lambda$ ). The coarse graining introduces difficulties in calculating these parameters from the microscopic interactions. Furthermore, even a first principles calculation of the microscopic interactions is highly nontrivial. For example, the anisotropy of the spins is believed to be due to a quantum exchange mechanism between layers that is not easily calculated or understood. Nevertheless, we can proceed by empirically searching through parameter space to find parameters in which the experimental results are observed.

In the region of parameter space in which the domain patterns and hysteresis loops have properties seen in the real experimental samples, the ferromagnetic coupling  $J$  and the anisotropy strength  $\alpha$  are approximately equal, whereas the dipole-dipole strength  $w$  is roughly an order of magnitude weaker. The competitive nature of these interactions give rise to interesting domain patterns and hysteresis loops [13, 14]. A strong  $\alpha$  tries to keep all spins pointing out of plane due to the weighting in the  $z$  direction. The positive  $J$  tries to maintain a local alignment of spins, thus large domains are favored by this energy term. Though weaker in magnitude per spin-spin interaction, the dipolar force is long range with an accumulated effect that competes significantly with the local couplings.

The amount of disorder in a system is determined by  $\lambda$ , with a large  $\lambda$  signifying low disorder. When  $\lambda = 1$ , the anisotropy energy is spherically symmetric (after averaging over many spins) and the system is no longer a perpendicular material. In addition to lowering  $\lambda$ , disorder also weakens the dipolar strength. Disorder in the real experimental systems exists in the interface between the Co and Pt layers. When disorder is large, the interface is highly non-planar, thus effectively suppressing the dipolar interaction after coarse graining. Though this disorder in the interface would most likely alter the relative strengths of  $J$  and  $\alpha$ , we remove this degree of freedom and set  $J = 0.85$  and  $\alpha = 0.875$  for all systems.

The low disorder systems have the most interesting domain patterns with labyrinthine mazes at remanence. The systems with the lowest amount of disorder studied have  $\lambda = 1000$  and  $w = 0.15$ . For this value of  $\lambda$ , the easy axes  $\hat{n}_i$  is almost parallel to  $\hat{z}$ . Starting at positive saturation, the large  $J$  and  $\alpha$  keep the spins aligned essentially vertically. But the dipole-dipole interaction is highly dissatisfied in this configuration. Because of this dissatisfaction, at a relatively high positive field, one or more small patches will flip.

Once a small “down” domain has formed in a sea of up spins, the local ferromagnetic interaction causes instabilities to occur at the boundary of the domain. Due to the ordered environment around the domain, the instabilities grow into lines. These configurations are long serpentine configurations in accordance with the recent experiments on Co/Pt films and also earlier experimental work [20]. The growth of the snakes is spontaneous, occurring at constant external field. Figure 2 shows the formation and growth of the snakes. In regions of high curvature, occasionally side branches grow and look very similar to experimental patterns. Due to the dipolar force, the domains behave as if they repel each other. This repulsion causes the growth to halt once the length of the snakes is comparable to the system size and the total area of negative spins fills a finite fraction of the sample. At this point, in order for more spins to flip, the field must be lowered.

The initial circular instability and subsequent growth occurs for a wide range of temperatures and therefore ap-

pears to be predominantly different from what one would expect if this was nucleation. If this was nucleation, near the critical field, domains would appear and disappear with a temperature dependent probability. Our simulations show that when a domain flips initially, it remains in that state above the critical field and never disappears. At the critical field a domain will quickly become unstable, even at zero temperature, and grows into serpentine patterns even with no change in applied field. The initial instability often occurs at the same location upon repeated field cycling which further indicates that this is not nucleation.

The growth of these snake-like domains is similar to what is seen in ferrofluids [17, 21, 23]. In that case however volume of fluid is conserved which means that the volume of fluid cannot spontaneously increase with external field. However the general shape of domains is similar, particularly their long serpentine shape ending with a wider head as shown by figure 2.

The growth at constant field introduces a cliff in the hysteresis loop; the growth of the snakes reduces the magnetization abruptly. Hysteresis curves of this type are shown in the first panel of figure 4. The end of this large avalanche signifies the point at which the snakes have taken up the available growth environment and are intertwined. After this point, the length of the snakes can no longer increase significantly but the width of the snakes does gradually increase by lowering the external field. Eventually, the field overcomes the repulsion and the snakes link and form a labyrinthine maze. Finally, the field will have a large negative value that saturates the spin in the negative  $z$  direction.

The systems with the highest amount of disorder studied have  $\lambda = 2$  and  $w = 0.05$ . With such a low weighting, the easy axes have large components in the plane that vary greatly from one spin to the next. Because the  $\hat{n}_i$ ’s no longer have a large probability of pointing in the  $z$  direction and the anisotropy energy is strong, the saturation magnetization is reduced. In other words, the spins tend to point along their easy axes which have larger in-plane components than the low disorder systems. This reduction of the saturation magnetization as disorder is increased is also seen in the experiments. Though the spins are more in-plane, the external field still starts at a large positive value, therefore the  $z$  component of the spins start positive. The weaker dipole coefficient requires more reduction of the field before the dipolar dissatisfaction causes a patch to flip, thus the remanent magnetization increases for more disordered systems.

Disorder causes the domains to have a rougher boundary. This rough edge is due to the more spherical symmetric easy axes of the spins at and near the edge. Furthermore, the highly irregular easy axes landscape prevents long snake-like domains from forming. Therefore, domains cannot grow significantly unless the external field is lowered. The stunting of the domain growth can be seen by a lack of any large avalanches seen in the hysteresis loop.

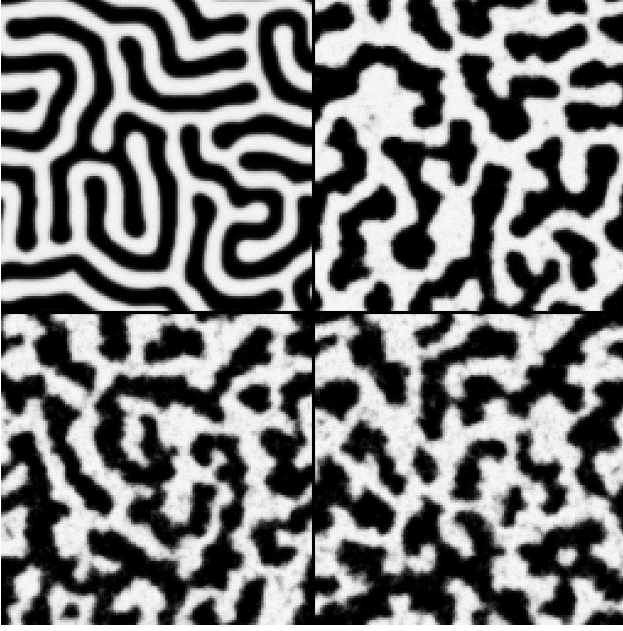


FIG. 3: Spin configurations at the coercive field for systems with different amounts of disorder. The systems with the least amount of disorder are in the upper left panel and greatest amount are in the lower right. The disorder parameters  $\lambda$  are 1000, 11, 4.1, 3 and the dipole strengths  $w$  are 0.15, 0.105, 0.08, 0.06.

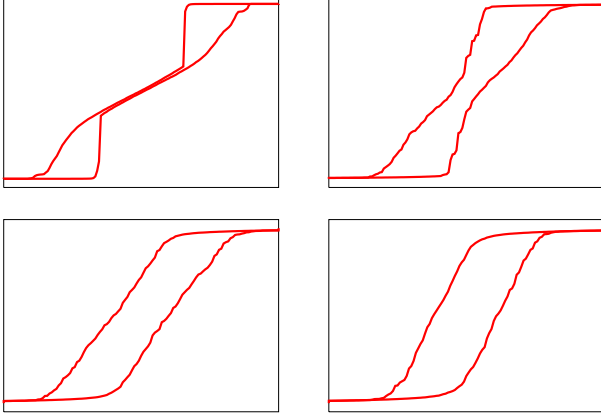


FIG. 4: Hysteresis loops for systems with different amounts of disorder; the vertical axes are the magnetizations and the horizontal axes are the external fields. The panels correspond to the same system as in figure 3. The cliff in the hysteresis curve vanishes as disorder is increased.

Figure 3 shows configurations near the coercive field for systems with increasing disorder. Figure 4 shows the corresponding hysteresis loops for these systems. The configurations and hysteresis plots are for systems with  $\lambda = 1000, 11, 4.1, 3$  and  $w = 0.15, 0.105, 0.08, 0.06$  starting from the upper left to the lower right panels. This se-

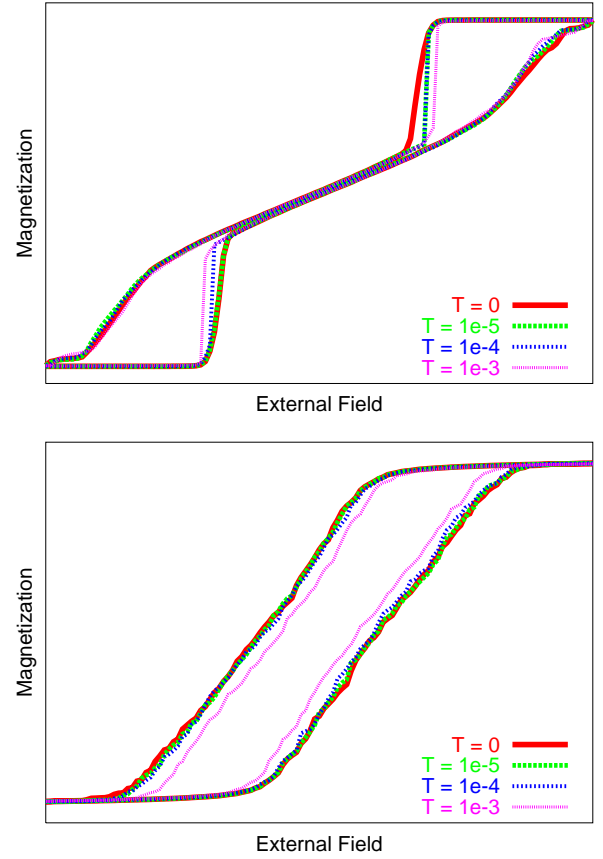


FIG. 5: Hysteresis loops at different temperatures for a low disorder system (top,  $\lambda = 1000, w = 0.15$ ) and a high disorder system (bottom,  $\lambda = 4.1, w = 0.08$ ). For both systems, thermal noise narrows the hysteresis loop. For the low disorder system, on the descending leg thermal noise causes the cliff to occur at a higher field.

quence of hysteresis plots shows how the height and slope of the cliff decreases as disorder increases. At an intermediate amount of disorder, snakes do grow but not to the extent of the entire system size. The domain growth is pinned by the disorder and growth cannot occur until the field is lowered. Eventually, beyond  $\lambda = 4.1$  and  $w = 0.08$ , there is no noticeable cliff in the hysteresis curve. A system with a lower  $w$  remains saturated for a larger range of external field, therefore the remanent magnetization and the width of the hysteresis loop increases as  $w$  decreases.

The general features of the domain patterns and hysteresis loops described above are dependent upon the amount of disorder but are independent of temperature for a wide range of temperature. However, thermal noise does affect the field in which the domains initially flip. This effectively narrows the hysteresis loops as shown in figure 5. Another study of Co-Pt multilayers shows this effect as well [22]. Though thermal noise does have an effect on the hysteresis loop, domain creation and growth



is not predominantly nucleation.

One can understand this by examining the low disorder system. Starting from positive saturation, at a critical field, circular initial domains and serpentine growth occurs for all temperatures. At zero temperature nucleation cannot occur, therefore the zero temperature critical field is analogous to the spinodal point. When thermal noise is present, it can cause domains to flip before the spinodal field is reached, thereby nucleating domains which then grow. Hence at finite temperature, the cliff occurs at a field larger than the zero temperature critical field (when all spins are initial saturated in the positive direction). But from figure 5, we see that this is not a strong effect. Nucleation only slightly changes the field in which the cliff occurs and is not the dominant phenomenon for domain formation and growth.

The qualitative features described in this section are observed in the experimental samples. In summary, low disorder systems have labyrinthine domain patterns and hysteresis loops with steep cliffs and high disorder systems have irregular patchy domains and more “standard” hysteresis loops.

## V. COVARIANCE RESULTS

As seen in the previous section, the amount of disorder and dipole strength dictates the type of domain patterns and hysteresis loops. In this section, we discuss how memory properties, specifically RPM and CPM, are determined by the amount of disorder. Though thermal noise did not have a large effect on the hysteresis loops and domain pattern, memory properties are highly sensitive to temperature.

At zero temperature, the snakes seen in the domain patterns of the low disorder systems meander due to the small differences in one direction versus another. These slight differences are mainly due to the randomness in the easy axes of the spins. Without thermal noise, every ascending leg will be identical to the next; a complete field cycle that saturates the magnet returns the system to exactly the same state. In other words, RPM is identically equal to unity.

Because the meandering is due to very slight differences in the local environment of the snake, thermal noise could alter the domain patterns dramatically. Even when the temperature is low, the domain configurations can be drastically different between points separated by an integral number of complete field cycles. In the second row of figure 6, two configurations of a low disorder system are so different that one could not tell that both panels are the same system separated by one field cycle. These two configurations both appear, at least visually, to have domains that are uncorrelated both in their positions and their shapes.

Of course high disorder systems are also affected by thermal noise. But because these systems are much more heterogeneous, a small amount of noise does not cause

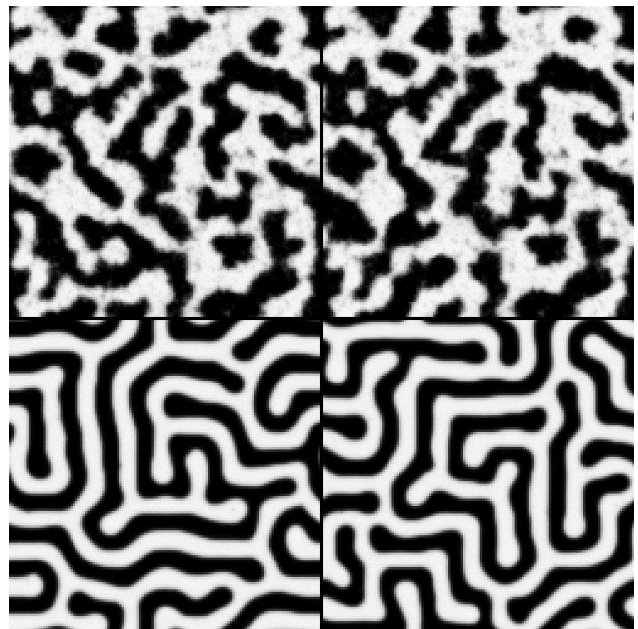


FIG. 6: Comparisons of the spin configurations after one complete cycle at the coercive field. The configurations on the top row are from a system with high disorder ( $\lambda = 4.1$  and  $w = 0.08$ ). Notice the domains have essentially the same shape and are in the same positions. The bottom two panels are configurations from a system with low disorder ( $\lambda = 1000$  and  $w = 0.15$ ). There does not appear to be any obvious correlation between the domains for the low disorder system. The temperature is  $10^{-5}$ .

such drastic differences. The lack of domain growth at constant field is due to the orientational disorder. This disorder also ensures that even for different realizations of thermal noise, the domains form in essentially the same locations with the same sizes. In other words, the relatively more reproducible growth of domains is another consequence of pinning by disorder. Therefore the differences in configurations after a complete field cycle, shown in the top row of figure 6, is not as drastic as was seen in the low disorder case.

Whereas thermal noise adequately explains return point differences, explanations of the differences between complementary points also require a discussion of the dynamics. When the precession term of the LLG equation is removed, the behavior of the complementary branch is identical to the return branch (with  $\mathbf{s} \rightarrow -\mathbf{s}$  and  $B_e \rightarrow -B_e$ ). But when precession is present, even at zero temperature, a configuration at field  $B$  along the ascending branch is not identical (after spin reversal) to the configuration at field  $-B$  along the descending branch.

As mentioned in the introduction, RPM and CPM quantify the amount of correlation between configurations. Because each system is saturated after every leg, RPM and CPM are independent of the number of intermediate field cycles. At very low temperatures, the covariance values for different legs essentially overlap. Fig-



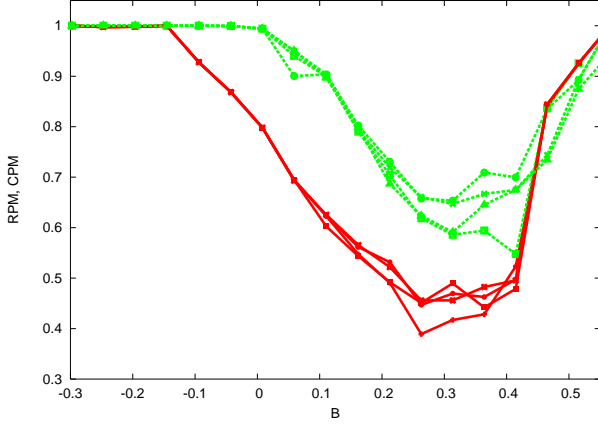


FIG. 7: RPM and CPM vs. external field for a  $\lambda = 4.1$  and  $w = 0.08$  system at a very low temperature of  $10^{-9}$ . The covariance values for four “return” legs (dashed lines) and four “complementary” legs (solid lines) are plotted. All “return” legs have essentially the same covariance. Similarly all “complementary” legs have the same covariance. Because the system reaches saturation at the end of every leg, RPM and CPM are independent of the number of intermediate field cycles.

Figure 7 shows RPM and CPM plots for a highly disordered system with  $\lambda = 4.1$  and  $w = 0.08$  at a very low temperature  $T = 10^{-9}$ . RPM is greater than CPM for most field points and the different RPM legs lie very close together as do the different CPM legs. This feature is seen in the experiments.

The effects of temperature on RPM and CPM are shown for a system with  $\lambda = 4.1$  and  $w = 0.08$  in figure 8. There are much larger fluctuations compared to the system in figure 7 due to the higher temperature. As expected, these fluctuations are reduced as the system size is increased. The average is done over many legs and the root mean square deviation is shown. These figures clearly show that at low temperature RPM is close to unity whereas CPM is significantly lower. As temperature increases, RPM decreases as discussed. Curiously, for low temperatures, within errors, CPM stays constant. Up to a temperature of  $\sim 10^{-4}$ , the dynamics appear to be dominant over temperature in terms of complementary point memory. This result emphasizes the importance of the vector dynamics. Furthermore, in the region with  $\text{RPM}, \text{CPM} < 1$  the amount of memory decreases with field. This decrease in memory with field is seen in the experiments as well.

For a temperature of  $10^{-4}$ , figure 9 shows the average RPM and CPM for systems with different amounts of disorder. The low disorder system has no significant amount of memory near the coercive field. Furthermore, a spike exists at the critical field where the instabilities initially form. This spike reveals the fact that the initial domain(s) forms at the same position after repeated field cycling, hence the large covariance. RPM and CPM

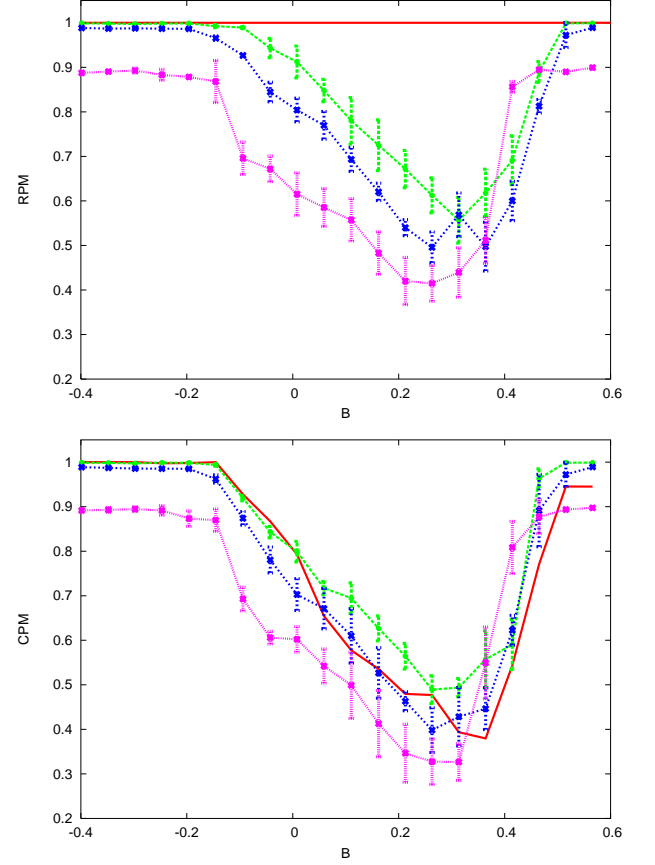


FIG. 8: RPM and CPM vs. external field for a highly disordered system ( $\lambda = 4.1$  and  $w = 0.08$ ) at different temperatures. At very large negative fields, temperature is inversely related to the height of the lines. The temperatures are  $T = 0, 10^{-5}, 10^{-4}, 10^{-3}$ . RPM and CPM values shown are the mean values for multiple field cycles with RMS error bars. The top panel shows how RPM is exactly equal to unity for zero temperature and decreases as temperature increases as expected. Unexpectedly, as shown in the bottom panel, CPM does not always decrease as temperature increases. In fact, except for the  $T = 10^{-3}$  case, CPM is essentially constant for all other temperatures within errors. Because CPM is similar between the zero and small temperature cases, thermal noise is not the dominant cause of loss of complementary memory.

drop off sharply away from this critical field due to the thermal sensitivity of the domains. For  $\lambda \leq 4.1$  and  $w \leq 0.08$  both RPM and CPM are noticeably above zero at all fields. The general features of the RPM and CPM plots are related to the features of the hysteresis loops as seen in figure 4; systems with a cliff in the hysteresis loop have much smaller RPM and CPM than systems with more standard hysteresis loops.

To more clearly illustrate the relation between disorder and memory, figure 10 contains a plot of RPM and CPM versus “disorder” at the coercive field. “Disorder” is quantified by  $1/\lambda$ . There is a definite increase in memory as the amount of disorder is increased. Both RPM

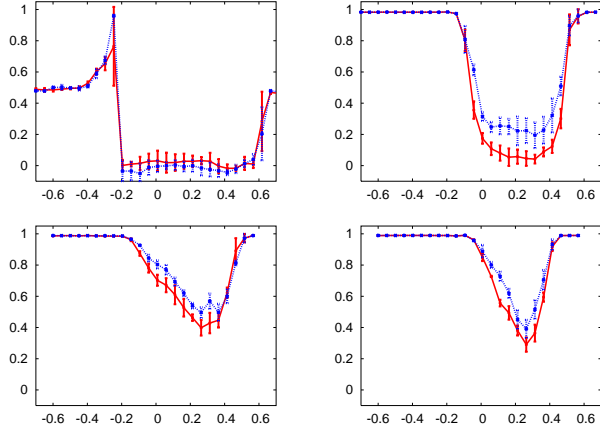


FIG. 9: RPM and CPM vs. external field as disorder is increased. The panels here refer to the same systems as in figure 3 and figure 4. The solid line represents CPM and the dashed line represents RPM. All panels have  $RPM > CPM$  except in the lowest disorder system where RPM and CPM are essentially equal. As disorder increases, both RPM and CPM increase. The difference between RPM and CPM is also more evident with a larger amount of disorder.

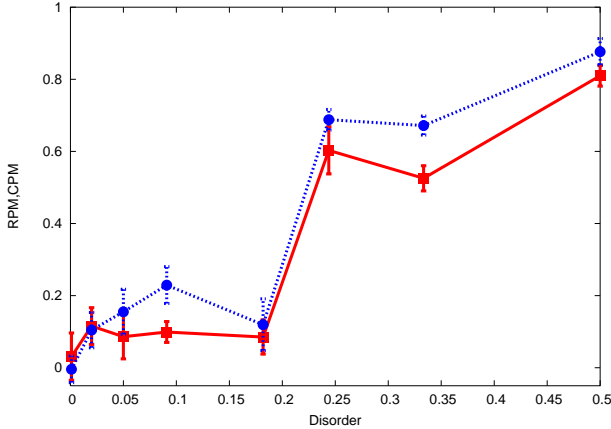


FIG. 10: RPM and CPM vs. “disorder” ( $1/\lambda$ ) at the coercive point. The squares represent CPM and the circles represent RPM. The increase in “memory” with disorder is evident.

and CPM are substantial for systems with  $\lambda \gtrsim 4.1$  which corresponds to the point where the snakes no longer appear in the domain patterns and the cliff no longer appears in the hysteresis loop. Similarly, the speckle experiment found that this point is where the amount of memory is considerable.

## VI. CONCLUSIONS

The experiments of ref. [11, 12] contain numerous observations of the domain patterns, hysteresis loops, and

memory properties of disordered Co/Pt multilayer thin films using a variety of techniques. In this paper, we have attempted to understand these results by numerically simulating the experimental systems. We have provided a plausible explanation for all of the results found and in particular counter-intuitive results on memory asymmetry upon field reversal. We have shown that vector dynamics can be crucial in the memory property of magnetic spin systems, without which our model would not be able to explain the experimental results.

Our simulations contain much of the qualitative features of the domain patterns and hysteresis loops. The domain patterns for systems with low disorder for both experiment and simulation are labyrinthine mazes at the coercive field. Furthermore, we observe snake-like growth of the domains which are responsible for the cliffs seen in the hysteresis loops in accord with experiment. As the amount of disorder in the system increases, irregular patches replace the serpentine domain patterns and the cliff in the hysteresis loop disappears. Because these features in the simulation resemble the features observed in the experiments, we believe the parameters used in the simulation are close to the actual parameters. It would be interesting to further investigate the growth instability in the low disorder regime which should be similar in analysis to the ferrofluid case [17] but without conservation of mass. It would also be interesting to see to what extent the analysis of the dendrite problem can be carried over to this case [24, 25, 26].

We have found that how thermal noise affects the different domain structures determines how well the system “remembers.” At finite temperature, the low disorder systems become uncorrelated much more easily than the high disorder systems; disorder tends to pin domains, thereby enabling the system to remember its past. The covariance behavior of RPM as disorder is varied in the simulations agree with much of the results from the experiments.

We are able to explain the seemingly paradoxical experimental result that complementary points appear to “forget” more than return points despite being governed by a Hamiltonian that is invariant upon  $\mathbf{s} \rightarrow -\mathbf{s}$  and  $B_e \rightarrow -B_e$ . The non-invariance of the LLG dynamical equation provides a natural explanation for this unexpected behavior. Spin precession reveals itself by decreasing the correlation between opposite legs. Because of the importance of precession for certain physical phenomena, scalar theories are inadequate even for highly anisotropic materials. From these simulation results, we show that the dynamic mechanism is able to explain, at least qualitatively, the observations from the speckle experiments. To make this more quantitative, a better experimental understanding of the sputtered films is needed.

Prior to this work, Jagla [13, 14] produced simulations with domain patterns and hysteresis loops remarkably similar to the experimental ones. In the first of his two papers [13], Jagla used a long range scalar  $\phi^4$  model and obtained domain patterns very similar to a large number

of different experiments. A  $\phi^4$  theory however is not able to reproduce major hysteresis loops correctly because  $\phi$  grows indefinitely with applied field.

In his second paper, Jagla [14] used a modified model that did not allow the indefinite growth of  $\phi$  and therefore can produce hysteresis curves that saturate. His model Hamiltonian contained all the terms used here: dipolar interaction, local elastic energy, perpendicular anisotropy, and an external field term. And like our work, disorder was introduced in the anisotropy. However, there are two major differences between Jagla's model and ours. The first difference is that Jagla's model in [14] was at zero temperature and therefore could not make predictions on the temperature or disorder dependence of RPM and CPM. The second more important difference is Jagla's use of a scalar model versus our vector model. Obviously, a scalar model cannot have precession, therefore the mechanism we propose here to explain RPM > CPM cannot be applied. And since there are no non-bilinear terms in this model (such as a random field term), there is no mechanism for RPM to be unequal to CPM. However, the scalar model does produce domain patterns and hysteresis loops similar to experiments.

Jagla also showed that when a small random field term is included in the Hamiltonian of his original  $\phi^4$  scalar model, instead of a random anisotropy, RPM is greater

than CPM [12] and the scalar model succeeds in explaining many of the features of the speckle data even with a relatively small field. But an important question remains: whether or not there exists a scalar theory that is capable of explaining simultaneously all of the features of the experiment that we are able to do with our vector model.

If our explanation turns out to be correct, this also has strong implications for theory, which has often ignored the vector nature of the dynamics and used scalar theories such as Ising models and  $\phi^4$  theories to understand these kind of systems. This opens up the possibility that there are other unexplored consequences of this lack of symmetry of the dynamical equation.

### Acknowledgments

We thank Conor Buechler, Eric Fullerton, Olav Hellwig, Steve Kevan, Kai Liu, Michael Pierce, and Larry Sorensen for the details and explanations of their experiment. We thank Eduardo Jagla, Onuttom Narayan, and Gergely Zimanyi for very useful discussions. We also thank Steve Kevan, Michael Pierce, and Larry Sorensen for careful readings of the manuscript.

- 
- [1] H.Barkhausen, Z. Phys. **20**, 401 (1919).
  - [2] P.J. Cote and L.V. Meisel, Phys. Rev. Lett. **67** 1334 (1991).
  - [3] L.V. Meisel and P.J. Cote, Phys. Rev. B **46** 10822 (1992).
  - [4] B. Alessandro, C. Beatrice, G. Bertotti, and A. Montorsi, J. Appl. Phys. **68** 2901 (1990); *ibid.* **68** 2908 (1990).
  - [5] J.S. Urbach, R.C. Madison, and J.T. Markert, Phys. Rev. Lett. **75** 276 (1995).
  - [6] O. Narayan, Phys. Rev. Lett. **77** 3855 (1996).
  - [7] S. Zapperi, P. Cizeau, G. Durin, and H.E. Stanley, Phys. Rev. B **58** 6353 (1998).
  - [8] G. Durin and S. Zapperi, Phys. Rev. Lett. **84** 4705 (2000).
  - [9] J.P. Sethna, K. Dahmen, S. Kartha, J.A. Krumhansl, B.W. Roberts and J.D. Shore, Phys. Rev. Lett. **70**, 3347 (1993).
  - [10] *Magnetic Recording Technology*, 2nd ed., edited by C. D. Mee and E. D. Daniel (McGraw-Hill Professional, New York 1996).
  - [11] M.S. Pierce, R.G. Moore, L.B. Sorensen, S.D., Kevan, O. Hellwig, E.E. Fullerton, and J.B. Kortright, Phys. Rev. Lett. **90**, 175502 (2003).
  - [12] M.S. Pierce, C.R. Buechler, L.B. Sorensen, J.J. Turner, S.D. Kevan, E.A. Jagla, J.M. Deutsch, T. Mai, O. Narayan, J.E. Davies, K. Liu, J. Hunter Dunn, K.M. Chesnel, J.B. Kortright, O. Hellwig, and E.E. Fullerton, Phys. Rev. Lett. **94**, 017202 (2005); and private communications.
  - [13] E.A. Jagla, Phys. Rev. E **70**, 046204 (2004).
  - [14] E.A. Jagla, cond-mat/0412461.
  - [15] J.M. Deutsch, T. Mai and O. Narayan, cond-mat/0408158, accepted for publication in Phys. Rev. E.
  - [16] F.H. de Leeuw, R. van den Doel and U. Enz, Rep. Prog. Phys. **43**, 689 (1980).
  - [17] S.A. Langer, R.E. Goldstein and D.P. Jackson, Phys. Rev. A **46**, 4894 (1992).
  - [18] G.M. Sandler, H.N. Bertram, T.J. Silva, and T.M. Crawford, J. Appl. Phys. **85**, 5080 (1999).
  - [19] A. Lyberatos, G. Ju, R.J.M. van de Veerdonk, and D. Weller, J. Appl. Phys. **91**, 236 2002.
  - [20] M. Seul, L.R. Monar, L. O'Gorman, and R. Wolfe, Science **254**, 1616 (1991).
  - [21] A.J. Dickstein, S. Erramilli, R.E. Goldstein, D.P. Jackson, and S.A. Langer, Science **261** 1012 (1993).
  - [22] D.L. Mobley, C.R. Pike, J.E. Davies, D.L. Cox, and R.P. Singh, J. Phys. (Cond Mat) **16** 5897 (2004)
  - [23] J.A. Miranda and M. Widom, Phys. Rev. E **55** 3758 (1997).
  - [24] J.S. Langer, Rev. Mod. Phys. **52** 1 (1980).
  - [25] A. Barbieri, D.C. Hong, and J.S. Langer, Phys. Rev. A **35** 1802 (1987).
  - [26] M.N. Barber, A. Barbieri, and J.S. Langer, Phys. Rev. A **36** 3340 (1987); *ibid.* **36** 3350 (1987).
  - [27] Sethna's definition of return point memory refers to systems that have the property that their spins will return to exactly the same configuration after an excursion of the external field away from and then back to its original value. The excursion cannot exceed the maximum and minimum values that had already been taken by the field.
  - [28] The actual experimentally measured quantity differs

from Eq. (3) slightly, because the average intensities depend on  $k$  and so the formula needs to be suitably

weighted. see [11, 12] for details.